Experimental investigation of high-efficiency weak-value amplification of nonunitary evolution

Zhi-Peng Li, Yi-Tao Wang,* Shang Yu, Wei Liu, Yu Meng, Yuan-Ze Yang, Zhao-An Wang, Nai-Jie Guo, Xiao-Dong Zeng, Jian-Shun Tang,† Chuan-Feng Li,‡ and Guang-Can Guo

CAS Key Laboratory of Quantum Information, University of Science and Technology of China, Hefei, Anhui 230026, China;
CAS Center for Excellence in Quantum Information and Quantum Physics, University of Science and Technology of China, Hefei, Anhui 230026, China;
and Hefei National Laboratory, University of Science and Technology of China, Hefei, Anhui 230088, China

(Received 31 May 2022; accepted 7 July 2022; published 20 July 2022)

High-sensitivity metrology plays an important role in parameter estimation, and weak-value amplification is a significant tool used to enhance sensitivity. However, the efficiency of weak-value amplification is always affected by the postselection probability and meter loss. In this article we report on the realization of a device for weak interaction that realizes the nonunitary evolution based on a spatial light modulator and applies the weak-value amplification of nonunitary evolution. The weak-value amplification of nonunitary evolution can achieve efficiency nearly ninefold that of unitary evolution experimentally under specific settings, because of the quadratic relation between the meter shift and the norm of the weak value $|A_w|$. This work demonstrates the superiority of nonunitary evolution in weak-value amplification, provides an experimental scheme of weak interaction for other forms of nonunitary evolution, and possesses the potential to be combined with other techniques for higher efficiency.

DOI: 10.1103/PhysRevA.106.012608

I. INTRODUCTION

The concept of weak-value amplification was first introduced into precision metrology by Aharonov *et al.* [1]. With the appropriate preselection state and postselection state, the parameter associated with the weak interaction between the system and meter can be estimated by the meter-state shift and amplified by the postselection strength. Compared to traditional measurement methods, weak-value amplification can provide many experimental advantages [2,3], e.g., better experimental sensitivity. Therefore, the method of weak-value amplification has been employed in estimation for a variety of physical parameters, such as phase [4–6], velocity [7], frequency [8], optical rotation [9], magneto-optical constant [10], beam deflection [11], temperature [12], Kerr nonlinearity [13], and the spin Hall effect of light [14].

However, the higher efficiency of weak-value amplification generally requires the larger weak value, i.e., the lower postselection probability [1]. Experimentally, postselection always leads to the reduction of the detected meter number and limits the measurement precision affected by the shot noise of the meter [15]. Therefore, achieving a larger amplification factor using the limited weak value is especially significant in the parameter estimation. Recently, it was indicated theoretically that the nonunitary weak-value amplification could possess enhanced sensitivity [16]. Under the weak interaction of nonunitary evolution, the meter state obtains a parameter-dependent shift that is proportional to the square of the norm of the weak value. Thus, the weak-value amplification of nonunitary evolution can be more efficient than that of unitary evolution where the meter shift is proportional to the norm of the weak value. More information about the coupling coefficient between the system and meter will be collected, although the nonunitary evolution introduces loss, in contrast to the unitary evolution [16].

In this article we report on the realization of a device for weak interaction that realizes the nonunitary evolution based on a spatial light modulator (SLM), where the parameter-dependent shift of the meter is encoded on the spatial shift of the meter beam. For the different postselection probabilities and coupling coefficients, the spatial shift of the output meter is measured and the results match well with the theoretical prediction. The experimental results demonstrate that the weak-value amplification of nonunitary evolution is indeed more efficient, because of the quadratic relation between the spatial shift of the meter state and the norm of the weak value.

II. THEORY

The theoretical scheme of the weak interaction of unitary evolution is shown in Fig. 1(a). The input state is given by $|\psi_i(x)\rangle = |\psi_i\rangle\,\psi(x)$, where $\psi(x) \propto \exp(-\frac{(x-x_0)^2}{4\sigma^2})$ defines the meter state and $|\psi_i\rangle = (|0\rangle + |1\rangle)/\sqrt{2}$ defines the system preselection state. The parameter x is the spatial coordinate and $\{|0\rangle, |1\rangle\}$ are one-qubit eigenstates. The state undergoes a weak interaction where the system is coupled with the meter by the unitary evolution, and the weak interaction of unitary

*yitao@ustc.edu.cn
†tjs@ustc.edu.cn
‡cfli@ustc.edu.cn

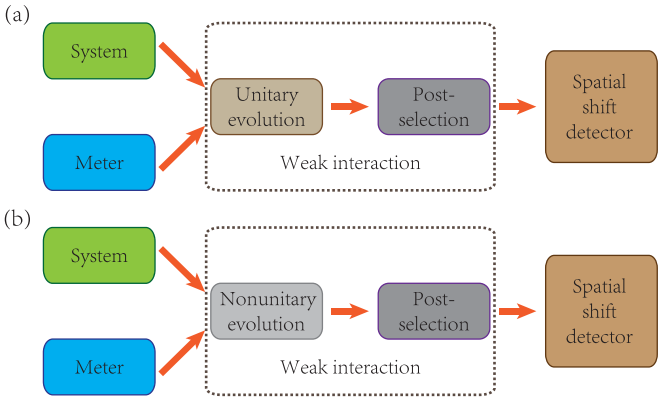

FIG. 1. Theoretical scheme of weak-value amplification. The input state consists of the system preselection state and meter state corresponding to the spatial profile of the input beam. (a) The system and meter state experience weak interaction of unitary evolution. Under the postselection, the intensity output will obtain a horizontal spatial shift that is linear with the norm of the weak value $|A_w|$. (b) The same system and meter state as in (a) experience the weak interaction of nonunitary evolution. Under the same postselection, the intensity output will obtain a horizontal spatial shift that is nonlinear, i.e., possesses the quadratic relation with the norm of the weak value $|A_w|$.

evolution is defined as

$$U_u = \begin{pmatrix} e^{-igx} & 0 \\ 0 & e^{igx} \end{pmatrix}. \tag{1}$$

The subscript u indicates unitary and g is the tiny parameter of interest which characterizes the interaction strength. With the system postselection state $|\psi_f\rangle = (|0\rangle - e^{-i\phi}|1\rangle)/\sqrt{2}$, which is nearly orthogonal to the preselection state, the intensity output can be deduced as

$$\begin{aligned} I_u(x) &\propto |\langle\psi_f| U_u |\psi_i\rangle \psi(x)|^2 \\ &\propto \sin^2\left(gx + \frac{\phi}{2}\right)\exp\left(-\frac{(x-x_0)^2}{2\sigma^2}\right). \end{aligned} \tag{2}$$

Considering that the parameter g is weak, i.e., $gx \ll 1$ and $g\sigma\cot(\frac{\phi}{2}) \ll 1$, the output can be written as

$$I_u(x) \propto \sin^2\left(\frac{\phi}{2}\right)\exp\left(-\frac{[x - x_0 - 2g\sigma^2\cot(\frac{\phi}{2})]^2}{2\sigma^2}\right). \tag{3}$$

Compared to the intensity input $I_i(x) \propto |\psi(x)|^2 = \exp(-\frac{(x-x_0)^2}{2\sigma^2})$, the intensity output obtains a horizontal spatial shift of $2g\sigma^2\cot(\frac{\phi}{2})$ which is linear with $\cot(\frac{\phi}{2})$. Consequently, the parameter g of interest can be estimated by measuring the spatial profile of the intensity output.

The weak value in this type of evolution can be deduced as

$$A_w = \frac{\langle\psi_f|A|\psi_i\rangle}{\langle\psi_f|\psi_i\rangle} = i\cot\left(\frac{\phi}{2}\right), \tag{4}$$

where $A = |0\rangle\langle 0| - |1\rangle\langle 1|$ is the one-qubit operation corresponding to the weak interaction. The postselection probability, i.e., the ratio of the overall output intensity to the input intensity of the meter, is $|\langle\psi_f|\psi_i\rangle|^2 = \sin^2(\frac{\phi}{2})$. When ϕ is smaller, the norm of the weak value $|A_w| = \cot(\frac{\phi}{2})$ and the profile shift of the intensity $2g\sigma^2\cot(\frac{\phi}{2})$ are larger. Nevertheless, the detected output meter will decrease with smaller ϕ. Therefore, the postselection phase ϕ should be chosen to balance.

In Fig. 1(b), the weak interaction of nonunitary evolution acting on the input state can be written as

$$U_n = \begin{pmatrix} e^{-\kappa} & 0 \\ 0 & 1 \end{pmatrix}, \tag{5}$$

where the subscript n indicates nonunitary and $\kappa \ll 1$ is also the parameter of interest that characterizes the weak interaction strength. With the same preselection state and postselection state, the intensity output can be deduced as

$$\begin{aligned} I_n(x) &\propto |\langle\psi_f| U_n |\psi_i\rangle \psi(x)|^2 \\ &\approx \sin^2\left(\frac{\phi}{2}\right)\exp\left[-\kappa + \frac{\kappa^2}{4}\cot^2\left(\frac{\phi}{2}\right)\right]\exp\left(-\frac{(x-x_0)^2}{2\sigma^2}\right). \end{aligned} \tag{6}$$

To deliver the parameter g to the spatial shift of the intensity profile, as shown in Eq. (3), the setting of $\kappa = \sqrt{4gx}$ can lead to the intensity output as [16]

$$\begin{aligned} I_n(x) &\propto \sin^2\left(\frac{\phi}{2}\right)\exp\left[-\sqrt{4gx} + gx\cot^2\left(\frac{\phi}{2}\right)\right] \\ &\quad\times\exp\left(-\frac{(x-x_0)^2}{2\sigma^2}\right) \\ &= \sin^2\left(\frac{\phi}{2}\right)\exp\left(-\frac{(x-x_0)^2}{2\sigma^2}\right) \\ &\quad\times\exp\left[gx\cot^2\left(\frac{\phi}{2}\right)\left(1 - \frac{\sqrt{4gx}}{gx\cot^2(\frac{\phi}{2})}\right)\right]. \end{aligned} \tag{7}$$

If $\sqrt{4gx} \ll gx\cot^2(\frac{\phi}{2})$ and $g\sigma\cot^2(\frac{\phi}{2}) \ll 1$, the output can be written as

$$I_n(x) \propto \sin^2\left(\frac{\phi}{2}\right)\exp\left(-\frac{[x - x_0 - g\sigma^2\cot^2(\frac{\phi}{2})]^2}{2\sigma^2}\right). \tag{8}$$

Obviously, the intensity output gains a horizontal spatial shift of $g\sigma^2\cot^2(\frac{\phi}{2}) \propto |A_w|^2$, which is nonlinear with $|A_w| = \cot(\frac{\phi}{2})$. Compared to the profile shift in the unitary-evolution situation [Eq. (3)], that in the nonunitary-evolution situation has an extra amplification factor of $\frac{1}{2}\cot(\frac{\phi}{2})$. Therefore, the weak-value amplification of nonunitary evolution has more advantages over that of unitary evolution for amplifying and estimating the parameter g because of its quadratic relation with the norm of the weak value $|A_w|$.

The relationship between the nonunitary coupling coefficient κ and the parameter g is selected as the square root relation $\kappa = \sqrt{4gx}$, aiming at delivering the weak interaction to the horizontal spatial shift of the intensity output as given in Eqs. (7) and (8). Whether the coefficient in front of gx is 4 or any other constant, the quadratic relation between the shift of nonunitary evolution $g\sigma^2\cot^2(\frac{\phi}{2})$ and the norm of the weak value $|A_w| = \cot(\frac{\phi}{2})$ will not change.

The square root relation in $\kappa = \sqrt{4gx}$ is significant and fundamental in our nonunitary weak-value amplification method. It is important to deliver the parameter g into the

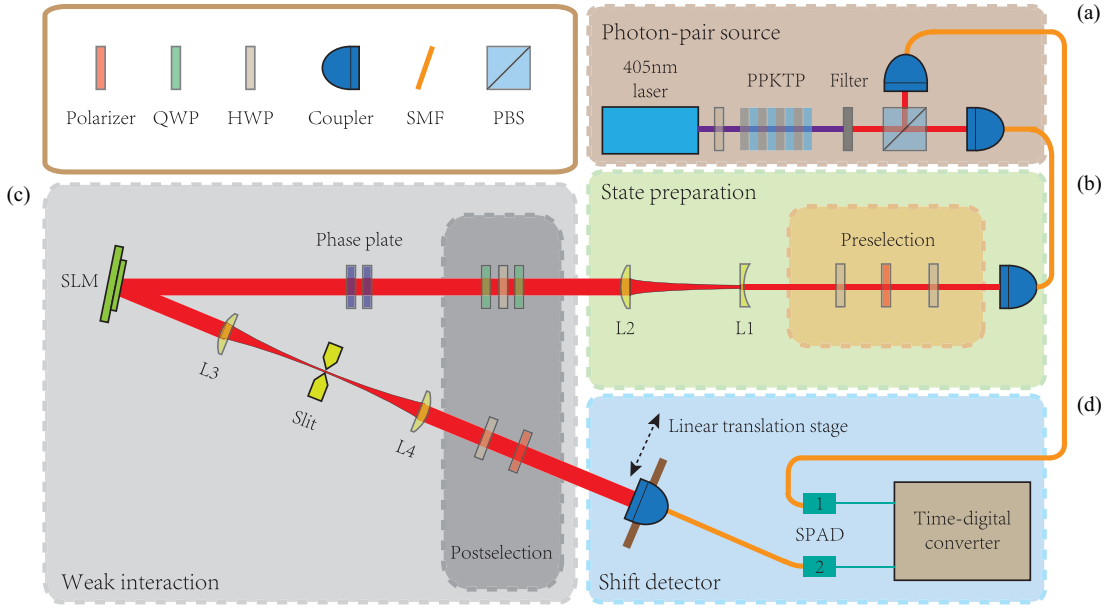

FIG. 2. Experimental setup. (a) Photon-pair source. The PPKTP crystal generates two photons simultaneously by spontaneous parametric down-conversion. The photon pairs are set as the target and trigger photons. (b) State preparation. Under the operations of the polarizer, HWPs, and lenses L1 and L2, the state with the appropriate spatial profile and correct polarization is prepared. (c) Weak interaction. The SLM, slit, and lenses L3 and L4 operate to realize controllable nonunitary evolution. The QWP, HWP, and polarizer form the postselection part. Two phase plates operate to compensate for the additional phase between $|H\rangle$ and $|V\rangle$. (d) Shift detector. The coupler and the linear transition stage transform the spatial shift of the beam to the intensity signal change. The time-digital converter analyzes the two signals detected by two SPADs. Here PBS denotes polarizing beam splitter.

meter state during the weak interaction while keeping the Gaussian spatial profile of the meter unchanged. If the square root relation $\kappa = \sqrt{4gx}$ and the weak-interaction conditions $\sqrt{4gx} \ll gx\cot^2(\frac{\phi}{2})$ and $g\sigma\cot^2(\frac{\phi}{2}) \ll 1$ are not satisfied, we probably cannot integrate the $\exp[-\kappa + \frac{\kappa^2}{4}\cot^2(\frac{\phi}{2})]$ part and the $\exp(-\frac{(x-x_0)^2}{2\sigma^2})$ part in Eq. (6) into the shifted Gaussian profile $\exp(-\frac{[x-x_0-g\sigma^2\cot^2(\frac{\phi}{2})]^2}{2\sigma^2})$ in Eq. (8) and further realize the nonunitary weak-value amplification. Therefore, the implementation of the square root relation between the coupling coefficient κ and the parameter g is crucial in devising the experimental scheme.

III. EXPERIMENT

To investigate the nonlinear weak-value amplification experimentally, we devised the experimental setup shown in Fig. 2, which consists of four parts.

Figure 2(a) shows the photon-pair source. Under the pump of the 405-nm laser, the periodically poled potassium titanyl phosphate (PPKTP) crystal generates the photon pair by spontaneous parametric down-conversion (SPDC). For the photon pair, one of them is regarded as the target photon for the following evolution and the other one is set as the trigger photon.

Figure 2(b) shows the state preparation. The beam of target photons is coupled into the single-mode fiber (SMF) for spatial pattern reshaping as the Gaussian profile. Then the beam passes through the polarizer and half waveplates (HWPs). The output polarization is set as $(|H\rangle + |V\rangle)/\sqrt{2}$. The lenses L1 and L2 operate to expand the beam profile. Specific to the experiment, the system qubit eigenstates $\{|0\rangle, |1\rangle\}$ are encoded on the polarization states, where $|H\rangle$ and $|V\rangle$ denote the horizontal and vertical polarization states, respectively. In this way, the state with appropriate polarization and spatial profile is prepared.

Figure 2(c) shows the weak interaction. Two quarter waveplates (QWPs) and one HWP work cooperatively to control the relative phase between $|H\rangle$ and $|V\rangle$, i.e., the phase ϕ in the postselection state. Two tilted phase plates whose optical axes are perpendicular to each other operate to compensate for the additional phase between $|H\rangle$ and $|V\rangle$. The SLM is the core device for the nonunitary evolution which consists of a two-dimensional liquid crystal array. Every liquid crystal unit in the array can add the adjustable phase to the local incident beam at $|H\rangle$. If the periodic phase with the spatial period Λ is applied to the SLM, such as $e^{i\,\mathrm{mod}(2\pi x/\Lambda, 2\pi)}$, it will work as a grating and introduce the diffraction effect for the incident beam [17]. Furthermore, the amplitude of the first-order diffraction beam can be modulated by the writing phase whose depth varies spatially on the SLM [17,18]. We set the phase pattern of the SLM as

$$M(m,n)\mathrm{mod}(F(m,n) + 2\pi m/\Lambda, 2\pi), \tag{9}$$

where (m,n) are the spatial coordinates on the SLM pattern and $F(m,n)$ and $M(m,n)$ are functions that depend on the desired amplitude and phase modulation. The input beam of $|H\rangle$ will be modulated by the function

$$T(m,n) = e^{iM(m,n)\mathrm{mod}(F(m,n)+2\pi m/\Lambda, 2\pi)}. \tag{10}$$

Based on the Taylor-Fourier expansion, the first-order diffraction beam is given by

$$T_1(m,n) = -\mathrm{sinc}[\pi M(m,n) - \pi]e^{i[F(m,n)+\pi M(m,n)]}, \quad (11)$$

where $\mathrm{sinc}(x) = \sin(x)/x$. If the desired amplitude and phase modulation have the form $Ae^{i\Phi}$, we set

$$A = \mathrm{sinc}(\pi M - \pi),$$
$$\Phi = F + \pi M. \quad (12)$$

Therefore, when the modulation functions $F(m,n)$ and $M(m,n)$ are given by

$$M = 1 + \frac{1}{\pi}\mathrm{sinc}^{-1}(A),$$
$$F = \Phi - \pi M, \quad (13)$$

the first-order diffraction beam $T_1(m,n)$ has the same form as $Ae^{i\Phi}$. The desired modulation is $Ae^{i\Phi} = e^{-\sqrt{4gx}}$ in our scheme, i.e., $A = e^{-\sqrt{4gx}}$ and $\Phi = 0$. Consequently, the modulation functions of the SLM pattern are given by

$$M(m,n) = 1 + \frac{1}{\pi}\mathrm{sinc}^{-1}(e^{-\sqrt{4gm}}),$$
$$F(m,n) = -\pi - \mathrm{sinc}^{-1}(e^{-\sqrt{4gm}}). \quad (14)$$

Here g is a controllable coefficient written on the SLM and can be set arbitrarily as needed. The square root relation between the coupling coefficient κ and the parameter g is satisfied by the modulation of the SLM.

Furthermore, by adding the additional global phase $e^{ik_x x + ik_y y}$ to the horizontal polarization part of the incident beam, the output $|H\rangle$ beam at the first order can move to the zeroth order. Finally, we can obtain one $|V\rangle$ beam at the zeroth order with unchanged amplitude and one $|H\rangle$ beam also at the zeroth order with a modulated amplitude of factor $e^{-\kappa(x)}$. The lenses L3 and L4 constitute a $4f$ system where the SLM, slit, and polarizer are all set at the focus point. The slit is used to block the other order diffraction beams and transmits the overlapped first-order $|H\rangle$ beam and zeroth-order $|V\rangle$ beam. Thus the SLM, lenses, and slit perform together to realize the desired weak interaction of nonunitary evolution on the $\{|H\rangle, |V\rangle\}$ basis. The HWP, polarizer, and QWP-HWP-QWP combination marked in Fig. 2 constitute the postselection.

Figure 2(d) shows the shift detector. The output beam through postselection is collected by the coupler with the SMF and then detected by the single-photon avalanche diode (SPAD). The coupler is placed on a linear translation stage that can move perpendicularly to the direction of beam propagation. The two translation-stage positions where the coupled intensity reaches the maximum with and without the SLM modulation can be detected; then the distance between them equals the horizontal spatial shift of the meter that we need to measure. The time-digital converter can count the detected photons coincident with the trigger photons detected by the other SPAD.

IV. RESULTS

To confirm the relation between the horizontal spatial shift of the intensity output and the postselection phase ϕ, we set $g = 0.5\ \mathrm{m}^{-1}$ and measured the spatial shift with ϕ changing from 6.4° to 12.0°. Moreover, the relation between the shift and the parameter g is also verified where $\phi = 6.4^\circ$ with g changing from $0.1\ \mathrm{m}^{-1}$ to $0.5\ \mathrm{m}^{-1}$. It should be mentioned that the diameter of the beam is set as $\sigma = 1466.3\ \mu\mathrm{m}$ so that the weak-value-amplification conditions $\kappa \ll 1$ and $4\tan^4(\frac{\phi}{2}) \ll g\sigma \ll \tan^2(\frac{\phi}{2})$ are satisfied.

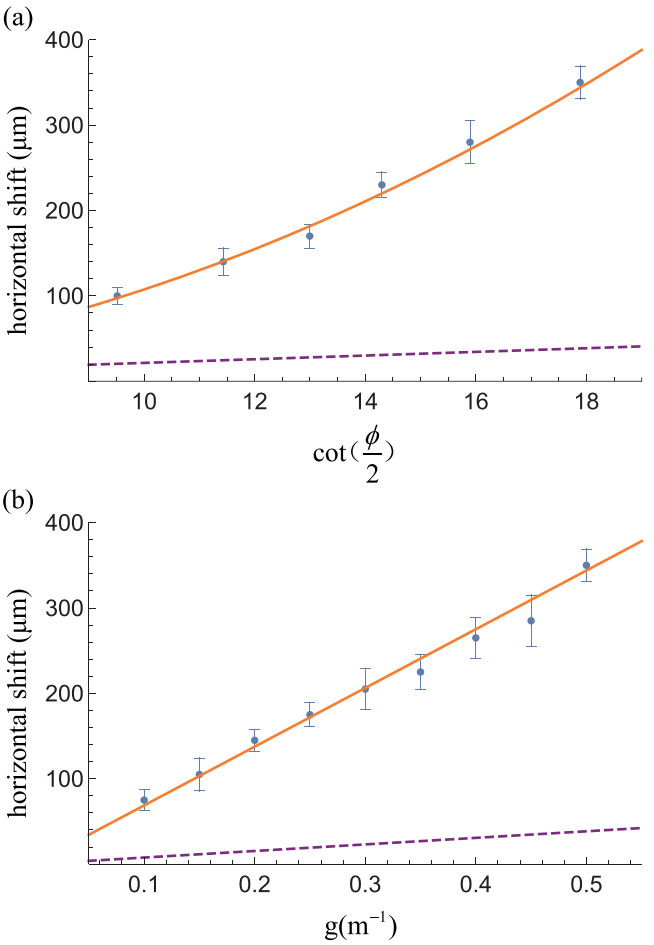

FIG. 3. The blue dots are the detected shift under nonunitary evolution. The orange solid line is the theoretical prediction under nonunitary evolution based on Eq. (8). The purple dashed line is the theoretical shift under unitary evolution based on Eq. (3). The error bars indicate the standard deviations of meter shifts which are derived by the Monte Carlo simulation method. (a) Relation between the horizontal spatial shift of the intensity output and the postselection phase ϕ with fixed $g = 0.5\ \mathrm{m}^{-1}$. The postselection phase ϕ varies from 6.4° to 12.0°, i.e., $|A_w| = \cot(\frac{\phi}{2})$ varies from 9.5 to 17.9. (b) Relation between the horizontal spatial shift of the intensity output and the parameter g with fixed $\phi = 6.4^\circ$. The parameter g varies from $0.1\ \mathrm{m}^{-1}$ to $0.5\ \mathrm{m}^{-1}$.

The experimental results are shown in Fig. 3. The blue dots are the detected shifts under nonunitary evolution. The orange solid line is the theoretical prediction under nonunitary evolution based on Eq. (8). The purple dashed line is the theoretical shift under unitary evolution based on Eq. (3). In Fig. 3(a), the norm of the weak value $|A_w| = \cot(\frac{\phi}{2})$ varies from 9.5 to 17.9 and then the detected shift under nonunitary evolution displays a nonlinear relationship to $\cot(\frac{\phi}{2})$. Experimentally, the shift of the output beam in the unitary-evolution

situation is too small to be detected because of its linearity with $\cot(\frac{\phi}{2})$. The shift under nonunitary evolution can reach nearly ninefold as large as that under unitary evolution and thus it can be detected clearly. Here the amplification factor 9 depends on the specific factor 4 inside $k = \sqrt{4gx}$ and the postselection parameter ϕ related to the nonlinear amplification of nonunitary evolution. In addition, we also study the relations between the output shift and the parameter g, under unitary and nonunitary evolution. In Fig. 3(b), the parameter g varies from 0.1 m^{-1} to 0.5 m^{-1} and both detected shifts are linear with the parameter g where the parameter variation can be amplified by the weak-value coefficient of $|A_w| = \cot(\frac{\phi}{2})$.

The results suggest that the nonlinear weak-value amplification of nonunitary evolution is more efficient than that of unitary evolution for amplifying and estimating the parameter g. Moreover, the SLM can apply any form of unitary or nonunitary evolution on the beam [17,18]. Thus, our experimental setup can be used for the investigation of weak-value amplification with other forms.

V. DISCUSSION

In contrast to the previous scheme of weak-value amplification where the output of interest is linear with the norm of the weak value $|A_w|$ [5,11], our work demonstrates the quadratic relation between the spatial shift of the intensity output and the norm of the weak value $|A_w|$. Therefore, for the same $|A_w|$, we can obtain a larger spatial shift of the intensity output by nonunitary evolution.

The weak-value amplification of nonunitary evolution can be applied to measure the other physical parameters, such as the rotation speed [16] and the liquid absorption coefficient as described below. Suppose an incident beam passes vertically through the liquid solution with a thickness of d. The intensity of the incident beam is I_0 and the absorption coefficient of the solution is α. Consequently, the intensity of the output beam is given by $I = I_0\exp(-\alpha d)$. If the thickness d of the liquid solution container in the parallel direction of the incident beam is designed as $d = \sqrt{Ax}$, where x is the spatial coordinate in the perpendicular direction of the incident beam and A is a parameter independent of x, the output intensity is deduced as $I(x) = I_0(x)\exp(-\alpha\sqrt{Ax}) = I_0(x)\exp(-\sqrt{A\alpha^2 x})$. Similar to the weak-value amplification of nonunitary evolution introduced above, we can obtain α under the relation $g = \frac{A}{4}\alpha^2$ by estimating the parameter g. Therefore, the absorption coefficient α of the liquid solution can be estimated by the weak-value amplification of nonunitary evolution. For this absorption-coefficient estimation, the probe light should always be restricted to weak light. Otherwise, the sample may be bleached by the probe light. In this case, the photon pairs from SPDC will be better than the attenuated laser with the same intensity by using coincidence counting to reduce noise.

For further developments, the power-recycling technique can be combined with the nonunitary evolution method to improve the precision of measurement in weak-value amplification [19]. The technique of entanglement-assisted weak-value amplification [20] could also be used to further enhance the efficiency of the detection of weak-value amplification. Consequently, our work has the ability to be applied to precision metrology for higher efficiency.

VI. CONCLUSION

We have proposed and constructed an experimental device for weak interaction between the system and meter state and demonstrated the weak-value amplification of nonunitary evolution. The nonunitary evolution that acts on the two eigenstates of a polarization qubit $\{|H\rangle, |V\rangle\}$ is realized based on the SLM. The weak-value amplification of nonunitary evolution is more efficient than that of unitary evolution for amplifying and estimating the parameter g because of the quadratic relation between the spatial shift of the intensity output and the norm of the weak value $|A_w|$. We measured the spatial shift of the intensity profile of the meter state experimentally for different postselection probabilities and coupling coefficients, and the shift in the nonunitary-evolution situation could reach up to nearly ninefold the displacement of that for unitary evolution under specific settings. The advantage of the nonunitary evolution over the unitary evolution in weak-value amplification was demonstrated experimentally in this work. Furthermore, our experimental scheme can be utilized for investigating the weak interaction for other forms of nonunitary evolution and possesses the potential to be combined with other techniques for higher efficiency.

ACKNOWLEDGMENTS

This work was supported by Innovation Program for Quantum Science and Technology (Grant No. 2021ZD0301200), the National Key Research and Development Program of China (Grant No. 2017YFA0304100), the National Natural Science Foundation of China (Grants No. 11674304, No. 11822408, No. 11774335, No. 11821404, No. 11904356, No. 12174370, and No. 12174376), the Key Research Program of Frontier Sciences of the Chinese Academy of Sciences (Grant No. QYZDY-SSW-SLH003), the Fok Ying-Tong Education Foundation (Grant No. 171007), the Youth Innovation Promotion Association of Chinese Academy of Sciences (Grants No. 2017492), Science Foundation of the CAS (Grant No. ZDRW-XH-2019-1), Anhui Initiative in Quantum Information Technologies (Grants No. AHY020100 and No. AHY060300), the Fundamental Research Funds for the Central Universities (Grants No. WK2470000026 and No. WK2470000028), and the Open Research Projects of Zhejiang Lab (Grant No. 2021MB0AB02).

[1] Y. Aharonov, D. Z. Albert, and L. Vaidman, How the Result of a Measurement of a Component of the Spin of a Spin-$\frac{1}{2}$ Particle Can Turn Out to be 100, Phys. Rev. Lett. **60**, 1351 (1988).

[2] G. I. Viza, J. Martínez-Rincón, G. B. Alves, A. N. Jordan, and J. C. Howell, Experimentally quantifying the advantages of weak-value-based metrology, Phys. Rev. A **92**, 032127 (2015).

[3] A. N. Jordan, J. Martínez-Rincón, and J. C. Howell, Technical Advantages for Weak-Value Amplification: When Less Is More, Phys. Rev. X **4**, 011031 (2014).

[4] C.-F. Li, X.-Y. Xu, J.-S. Tang, J.-S. Xu, and G.-C. Guo, Ultrasensitive phase estimation with white light, Phys. Rev. A **83**, 044102 (2011).

[5] X.-Y. Xu, Y. Kedem, K. Sun, L. Vaidman, C.-F. Li, and G.-C. Guo, Phase Estimation with Weak Measurement Using a White Light Source, Phys. Rev. Lett. **111**, 033604 (2013).

[6] X. Qiu, L. Xie, X. Liu, L. Luo, Z. Li, Z. Zhang, and J. Du, Precision phase estimation based on weak-value amplification, Appl. Phys. Lett. **110**, 071105 (2017).

[7] G. I. Viza, J. Martínez-Rincón, G. A. Howland, H. Frostig, I. Shomroni, B. Dayan, and J. C. Howell, Weak-values technique for velocity measurements, Opt. Lett. **38**, 2949 (2013).

[8] D. J. Starling, P. B. Dixon, A. N. Jordan, and J. C. Howell, Precision frequency measurements with interferometric weak values, Phys. Rev. A **82**, 063822 (2010).

[9] X. Qiu, L. Xie, X. Liu, L. Luo, Z. Zhang, and J. Du, Estimation of optical rotation of chiral molecules with weak measurements, Opt. Lett. **41**, 4032 (2016).

[10] X. Qiu, X. Zhou, D. Hu, J. Du, F. Gao, Z. Zhang, and H. Luo, Determination of magneto-optical constant of Fe films with weak measurements, Appl. Phys. Lett. **105**, 131111 (2014).

[11] P. B. Dixon, D. J. Starling, A. N. Jordan, and J. C. Howell, Ultrasensitive Beam Deflection Measurement via Interferometric Weak Value Amplification, Phys. Rev. Lett. **102**, 173601 (2009).

[12] H. Li, J.-Z. Huang, Y. Yu, Y. Li, C. Fang, and G. Zeng, High-precision temperature measurement based on weak measurement using nematic liquid crystals, Appl. Phys. Lett. **112**, 231901 (2018).

[13] G. Chen, N. Aharon, Y.-N. Sun, Z.-H. Zhang, W.-H. Zhang, D.-Y. He, J.-S. Tang, X.-Y. Xu, Y. Kedem, C.-F. Li, and G.-C. Guo, Heisenberg-scaling measurement of the single-photon Kerr non-linearity using mixed states, Nat. Commun. **9**, 93 (2018).

[14] O. Hosten and P. Kwiat, Observation of the spin Hall effect of light via weak measurements, Science **319**, 787 (2008).

[15] A. Nishizawa, K. Nakamura, and M.-K. Fujimoto, Weak-value amplification in a shot-noise-limited interferometer, Phys. Rev. A **85**, 062108 (2012).

[16] W.-T. Liu, J. Martínez-Rincón, and J. C. Howell, Weak value amplification for nonunitary evolution, Phys. Rev. A **100**, 012125 (2019).

[17] J. A. Davis, D. M. Cottrell, J. Campos, M. J. Yzuel, and I. Moreno, Encoding amplitude information onto phase-only filters, Appl. Opt. **38**, 5004 (1999).

[18] E. Bolduc, N. Bent, E. Santamato, E. Karimi, and R. W. Boyd, Exact solution to simultaneous intensity and phase encryption with a single phase-only hologram, Opt. Lett. **38**, 3546 (2013).

[19] Y.-T. Wang, J.-S. Tang, G. Hu, J. Wang, S. Yu, Z.-Q. Zhou, Z.-D. Cheng, J.-S. Xu, S.-Z. Fang, Q.-L. Wu, C.-F. Li, and G.-C. Guo, Experimental Demonstration of Higher Precision Weak-Value-Based Metrology Using Power Recycling, Phys. Rev. Lett. **117**, 230801 (2016).

[20] J.-S. Chen, B.-H. Liu, M.-J. Hu, X.-M. Hu, C.-F. Li, G.-C. Guo, and Y.-S. Zhang, Realization of entanglement-assisted weak-value amplification in a photonic system, Phys. Rev. A **99**, 032120 (2019).